AFRL-RI-RS-TR-2014-034

NEW METHODS OF ENTANGLEMENT WITH SPATIAL MODES OF LIGHT

COLGATE UNIVERSITY

FEBRUARY 2014

FINAL TECHNICAL REPORT

APPROVED FOR PUBLIC RELEASE; DISTRIBUTION UNLIMITED

STINFO COPY

AIR FORCE RESEARCH LABORATORY
INFORMATION DIRECTORATE

■ **AIR FORCE MATERIEL COMMAND** ■ **UNITED STATES AIR FORCE** ■ **ROME, NY 13441**

NOTICE AND SIGNATURE PAGE

Using Government drawings, specifications, or other data included in this document for any purpose other than Government procurement does not in any way obligate the U.S. Government. The fact that the Government formulated or supplied the drawings, specifications, or other data does not license the holder or any other person or corporation; or convey any rights or permission to manufacture, use, or sell any patented invention that may relate to them.

This report was cleared for public release by the 88th ABW, Wright-Patterson AFB Public Affairs Office and is available to the general public, including foreign nationals. Copies may be obtained from the Defense Technical Information Center (DTIC) (http://www.dtic.mil).

AFRL-RI-RS-TR-2014-034 HAS BEEN REVIEWED AND IS APPROVED FOR PUBLICATION IN ACCORDANCE WITH ASSIGNED DISTRIBUTION STATEMENT.

FOR THE DIRECTOR:

/ S /
PAUL M. ALSING
Work Unit Manager

/ S /
MARK H. LINDERMAN
Technical Advisor, Computing & Communications Division
Information Directorate

This report is published in the interest of scientific and technical information exchange, and its publication does not constitute the Government's approval or disapproval of its ideas or findings.

REPORT DOCUMENTATION PAGE

Form Approved
OMB No. 0704-0188

1. REPORT DATE *(DD-MM-YYYY)*	2. REPORT TYPE	3. DATES COVERED *(From - To)*
FEB 2014	FINAL TECHNICAL REPORT	OCT 2010 – SEP 2013

4. TITLE AND SUBTITLE

NEW METHODS OF ENTANGLEMENT WITH SPATIAL MODES OF LIGHT

5a. CONTRACT NUMBER
FA8750-11-2-0034

5b. GRANT NUMBER
N/A

5c. PROGRAM ELEMENT NUMBER

6. AUTHOR(S)

Enrique J. Galvez

5d. PROJECT NUMBER
T2QC

5e. TASK NUMBER
CO

5f. WORK UNIT NUMBER
LG

7. PERFORMING ORGANIZATION NAME(S) AND ADDRESS(ES)

Colgate University
13 Oak Drive
Hamilton, NY 13346-1388

8. PERFORMING ORGANIZATION REPORT NUMBER

9. SPONSORING/MONITORING AGENCY NAME(S) AND ADDRESS(ES)

Air Force Research Laboratory/RITA
525 Brooks Road
Rome NY 13441-4505

10. SPONSOR/MONITOR'S ACRONYM(S)
AFRL/RI

11. SPONSOR/MONITOR'S REPORT NUMBER
AFRL-RI-RS-TR-2014-034

12. DISTRIBUTION AVAILABILITY STATEMENT

Approved for Public Release; Distribution Unlimited. PA# 88ABW-2014-0535
Date Cleared: 14 Feb 14

13. SUPPLEMENTARY NOTES

14. ABSTRACT

The goal of this project is to produce entangled states of polarization and spatial mode. On the theoretical side, it involved the development of the mathematical formalism for a deep understanding of the modes that combine light's polarization with spatial mode. On the experimental side, this entailed the development, implementation and testing of laboratory techniques. The results include the development of new laboratory techniques to produce entanglement of polarization and spatial mode, the development of a new set of tailored optical beams, called Poincaré beams, and new measurements of single photons entangled in polarization and spatial mode.

15. SUBJECT TERMS

Quantum Computation, Entanglement, Polarization of light, Spatial modes

16. SECURITY CLASSIFICATION OF:			17. LIMITATION OF ABSTRACT	18. NUMBER OF PAGES	19a. NAME OF RESPONSIBLE PERSON
a. REPORT	b. ABSTRACT	c. THIS PAGE			**PAUL M. ALSING**
U	U	U	SAR	29	19b. TELEPHONE NUMBER (*Include area code*) **N/A**

TABLE OF CONTENTS

LIST OF FIGURES

1.0 SUMMARY

The goal of this project is to produce entangled states of polarization and spatial mode. On the theoretical side, it has signified the development of the mathematical formalism for a deep understanding of the modes that combine light's polarization with spatial mode. On the experimental side, this has entailed the development, implementation and testing of laboratory techniques to accomplish this goal.

Our results include the development of new laboratory techniques to produce entanglement of polarization and spatial mode. These efforts entail removing spatial mode impurities that are inherent in the technique to generate single photons, parametric down-conversion, to then encode polarization and desired spatial mode superpositions onto the light. These include quantum bits greater than two, such as qutrits, ququarts and ququints. The implementation of the encoding of these higher quantum spaces is non-trivial due to the decohering effects produced by the polarization interferometers that are needed to implement the polarization-spatial-mode entanglement. We devised several schemes to do these implementations, but the decohering effects in key components of the apparatus challenged us, forcing us to redesign them. After much development we devised and tested a novel common-path interferometer using one or two consecutive spatial light modulators, which introduce no decohering effects. Since then we have redeveloped our schemes to produce 2-photon 4-qubit states, then as a first step toward their full implementation, we have performed a first polarimetric measurement of the non-separable state of polarization and spatial mode on heralded single photons.

In the process of generating non-separable states of polarization and spatial mode of single photons, we studied the properties of the corresponding classical state, which had not been investigated before. Thus, an unanticipated result of this project is the development of a new set of tailored optical beams, called Poincaré beams. These are beams that contained all the states of polarization encoded in a single beam, as mappings of the Poincaré sphere onto it. There are parallel efforts in the optics research community to implement imaging devices that can decode images by polarization as well as intensity and wavelength. Our efforts contribute to the converse: encoding arbitrary polarization patterns in an optical beam. We do so not by manipulating the polarization of sections of an optical beam, but by manipulating combinations of spatial modes in distinct polarization states, a more fundamental approach. In doing so we discovered that we could access polarization patterns that had been studied theoretically, but not implemented in the laboratory. Our parallel work on this topic then focused on the study and generation of isolated polarization singularities, also known as C-points. We developed a theory and laboratory implementations of these novel optical features.

The results of this project provide fundamental as well as practical approaches to implement the encoding of high-dimensional quantum spaces on single photons and entangling them with partner photons. This will enable further implementation of quantum computing algorithms with photon pairs. This work also opened new approaches to encoding polarization and spatial mode in imaging, enhancing its dimensions with potential practical applications in sensing and communications.

2.0 INTRODUCTION

Polarization and imaging are mature topics in optics theory and technology. The merging of the two has been slow and is still in its early stages. The use of polarization in photon entanglement is quite extensive, but the use of spatial modes is less so due to technological challenges. Their combined modal space is neither well studied nor developed. Beyond the quantal regime, spatial modes and polarization are virtually divorced in an industry that today relies extensively on imaging, and to a lesser degree, on polarization. Yet there are research groups that are close to delivering a camera that decodes image as well as polarization [1]. When it arrives, we will be quite unprepared, as the technology that marries polarization and spatial mode needs much development. The topic of this project funded by the Air Force revolves around the integration of polarization and spatial mode. In the quantal domain, we investigated the creation of entanglement of polarization and spatial modes of photons, and in the classical domain we investigated the generation of optical beams in hybrid polarization-spatial modes. Due to the novelty of the problem we contributed with fundamental advances in the understanding of polarization-spatial modes, which are linked to the quantal entangled states in the single-photon limit.

Efforts to implement quantum computation are challenged by the practicalities of producing quantum bits, or qubits, that are entangled with each other. The implementation of qubits with light involves parametric down-conversion. The latter method is now quite accessible for the production of photon pairs. The expansion of this method to implement entanglement of more than two photons has been demonstrated but is quite challenging. Parallel ongoing efforts at Air Force Rome Labs entail expanding entanglement to four polarization entangled photons in a novel way [2,3]. Thus, increasing the number of qubits by just increasing the number of photons is not the best route to implementing quantum computation with many qubits. In this project we investigate increasing the number of qubits per photon. Polarization is the common means for implementing photon qubits because the technology to implement and measure polarization states is quite mature. Indeed the first demonstrations of quantum entanglement were done via polarization [4]. However, polarization encompasses only a 2-dimensional space. An additional degree of freedom is spatial mode. Spatial-mode entanglement comes naturally in parametric down-conversion via conservation of orbital angular momentum [5]. However, this entanglement cannot be easily adjusted. Previous reports of spatial-mode entanglement rely on the entanglement provided by parametric down-conversion [6,7,8]. One research group uses an electro-optical device to insert low-order spatial modes [9]. The goal of our project is to control the spatial entanglement to encode any mode and combine it with polarization to increase the number of qubits per photon. Our efforts toward this end are outlined in this report.

Entangled states involve non-separable superpositions of quantum states. The classic Bell state for two polarization-entangled photons is, written in the Dirac notation,

$$|\psi\rangle = {}^{1}\!/_{\sqrt{2}}\,(|\mathrm{H}\rangle_1|\mathrm{H}\rangle_2 + |\mathrm{V}\rangle_1|\mathrm{V}\rangle_2) \qquad (1)$$

Where *H* and *V* denote the horizontal and vertical states of linear polarization and the subindices denote the photon label. The nonseparability of Eq. (1) signifies that we cannot factorize the state such that it can be expressed as a product state of the polarization state of each photon. If we now

consider a single photon with spatial and polarization degrees of freedom we can equally have a nonseparable state:

$$|\psi\rangle = {}^{1}/_{\sqrt{2}}\,(|H\rangle|u_A\rangle + |V\rangle|u_B\rangle) \tag{2}$$

where u_A and u_B represent orthogonal spatial modes. Equation (2) does not involve nonlocality, but at the quantum level it constitutes a form of entanglement. The important feature of spatial modes is that they form an infinite space; images are superposition of spatial modes. Thus, tapping on to them promises advances in information carrying capacity and computation [10].

The study of polarization-spatial superpositions has been slow because they had not been seen as viable or valuable technologies. Thus, they had not been well studied at a fundamental level. This also had to do with the lack of technologies involved in accessing individual spatial modes. Earliest work on hybrid modes of polarization and spatial mode involved passive optical elements, which were used for generating "vector" beams [11,12], which are beams with a transverse profile containing linear states of polarization of varying orientation following some pattern, such as radial or azimuthal. The advent of spatial light modulators, active electro-optical elements, changed this situation, making the encoding and decoding of spatial modes much more easier [8,13]. Implementations of Eq. (2) with coherent states (i.e. laser beams) with arbitrary spatial modes gave rise to "Poincare" beams, which carry single or multiple mappings of the Poincare sphere onto the beam profile. These modes also contain optical singularities, which are points or lines where a parameter of the field is singular or undefined [14]. For example, polarization singularity C-points are points of circular polarization surrounded by a field of polarization ellipses whose orientation rotates as a function of the angle about the C-point [15]. Thus, the point is singular in polarization orientation. Investigation of these optical features is important for understanding and diagnosing polarization and spatial modes.

3.0 METHODS, ASSUMPTIONS, AND PROCEDURES

3.1. Production of 2-photon 4-qubit cluster states

Photon pairs produced by parametric down-conversion are in an entangled state of spatial modes, due to conservation if orbital angular momentum [16]:

$$|\psi_S\rangle = \sum_\ell c_\ell |u_\ell\rangle_1 \,|\, u_{\ell_p-\ell}\rangle_2, \tag{3}$$

where the pump photon has orbital angular momentum $l_p\hbar$ and due to conservation of orbital angular momentum, the down converted photons have angular momentum $\ell\hbar$ and $(l_p-\ell)\hbar$. Coefficients c_ℓ depend on the focusing of the pump laser incident of the down-conversion crystal, and where $c_0 > c_1 > c_2 > \cdots$ when $\ell_p = 0$. Unfortunately, it is not easy to change the values of c_ℓ, and thus it is not easy to create a state that is a superposition of only desired spatial modes. We have proposed two methods to do this [17,18]. Both involve projecting the state of the photons onto the fundamental mode. That is, reducing the spatial state of the light to a product state of the fundamental spatial modes (i.e., with $\ell = 0$).

To create a cluster state of polarization and spatial mode of two photons we have the scheme shown in Fig. 1. The starting point is to generate polarization-entangled photons via standard techniques. We do so using the two BBO crystal technique [19], generating the state of Eq. (1). Once the photons are in free space they pass through single-mode fibers, putting the pairs in the state

$$|\psi\rangle = {}^{1}/_{\sqrt{2}}(|\mathrm{H}\rangle_1|\mathrm{H}\rangle_2 + |\mathrm{V}\rangle_1|\mathrm{V}\rangle_2)|\mathrm{u}_{00}\rangle_1|\mathrm{u}_{00}\rangle_2 \tag{4}$$

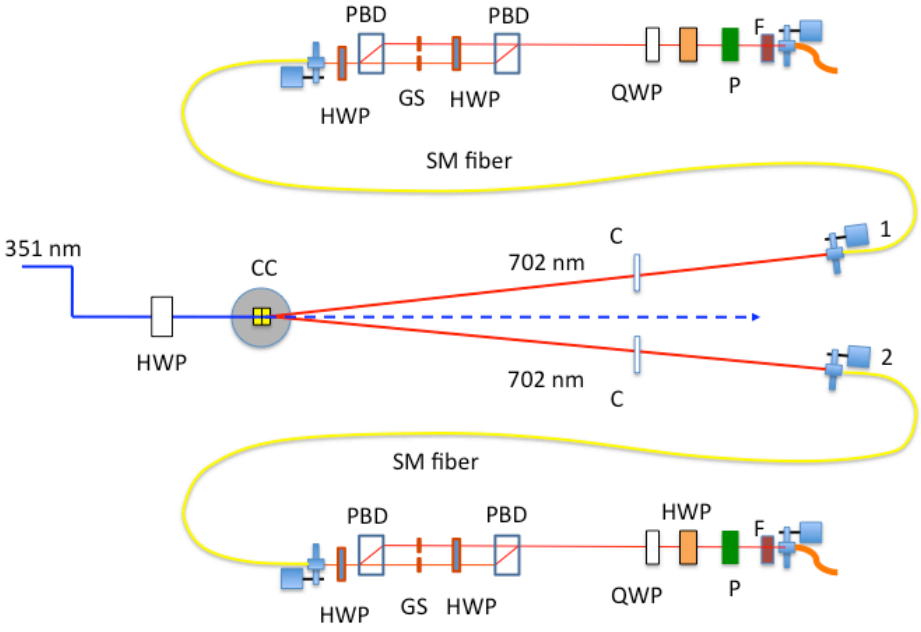

Figure 1. Apparatus for a proposed generation of cluster states of two photons. Optical elements include: half-wave plate (HWP), crystal (CC), compensating crystals (C), single mode (SM) fibers, quarter-wave plate (QWP), polarizing beam displacer (PBD), polarizer (P), glass slide (GS), band-pass filter (F).

Past the single-mode fiber the light is launched onto a polarization interferometer. Figure 1 shows the first apparatus that we investigated for introducing spatial modes. A polarizing beam displacer split the light entering the interferometer: vertically polarized light continued straight and horizontally polarized light was displaced. Glass slides in each arm imparted Hermite-Gauss spatial modes HG_{10} and HG_{01} on the vertical and horizontal components, respectively. A half-wave plate and a second beam splitter completed the interferometer. The state of polarization of the second photon (2) was rotated by 45 degrees, effecting the transformations:

$$|H\rangle \rightarrow |D\rangle = {}^{1}/_{\sqrt{2}}(|H\rangle + |V\rangle) \tag{5}$$

and

$$|V\rangle \rightarrow |A\rangle = {}^{1}/_{\sqrt{2}}(-|H\rangle + |V\rangle) \tag{6}$$

Past the interferometers the light was in the state

$$|\psi'\rangle = {}^{1}/_{2}\,(|\mathrm{H}\rangle_1|\mathrm{D}\rangle_2 + |\mathrm{V}\rangle_1|\mathrm{A}\rangle_2)|\mathrm{u}_{00}\rangle_1|\mathrm{u}_{00}\rangle_2 \tag{7}$$

or, replacing relations (5) and (6), we get

$$|\psi'\rangle = {}^{1}/_{\sqrt{2}}\,(|\mathrm{H}\rangle_1|\mathrm{H}\rangle_2 + |\mathrm{H}\rangle_1|\mathrm{V}\rangle_2 - |\mathrm{V}\rangle_1|\mathrm{H}\rangle_2 + |\mathrm{V}\rangle_1|\mathrm{V}\rangle_2)|\mathrm{u}_{00}\rangle_1|\mathrm{u}_{00}\rangle_2 \tag{8}$$

This is the state of the light just before the interferometers. Via the polarization interferometers, spatial modes were encoded according to the state of polarization:

$$|H\rangle|u_{00}\rangle \rightarrow |H\rangle|u_{10}\rangle = |H, u_{10}\rangle \tag{9}$$

and

$$|V\rangle|u_{00}\rangle \rightarrow |V\rangle|u_{01}\rangle = |V, u_{01}\rangle, \tag{10}$$

where we have introduced a more efficient notation. The interferometers transform the state of the two photons to:

$$|\psi''\rangle = {}^{1}/_{2}\,(|\mathrm{H}, u_{10}\rangle_1|\mathrm{H}, u_{10}\rangle_2 + |\mathrm{H}, u_{10}\rangle_1|\mathrm{V}, u_{01}\rangle_2 - |\mathrm{V}, u_{01}\rangle_1|\mathrm{H}, u_{10}\rangle_2 + |\mathrm{V}, u_{01}\rangle_1|\mathrm{V}, u_{01}\rangle_2), \tag{11}$$

which has the same form as the linear cluster state:

$$|\psi''\rangle = {}^{1}/_{2}\,(|0000\rangle + |0011\rangle - |1100\rangle + |1111\rangle) \tag{12}$$

The state given by Eq. (12) can be used for some basic forms of quantum computation.

3.2 Encoding any desired mode

The glass slides of Fig.1 were the starting point. We then moved to implement spatial light modulators for encoding spatial modes. The schemes of Figs. 2, 3 and 4 show our iterations. The one in Fig. 2 separates the light by polarization, with the mode associated to each state reaching half pane of the spatial light modulator (SLM). This scheme was inspired in a previously reported design [13]. The SLM had phase-blazed gratings programmed onto it, encoding the desired spatial mode. The insert to the figure shows an example of the programming of the spatial light modulator. We had to use half-wave plates to rotate the polarization of the light, as the SLM's phase-encoded pattern only affects vertically-polarized light.

The interferometer of Fig. (2) works well with light that has a coherence length of a few millimeters, but not with the broadband light produced by parametric down-conversion. The advantage of the grating encodings is that only the desired modes are encoded in the selected first-order diffraction direction. This avoids any contamination produced by specular reflection off the front of the SLM and diffraction due to the pixilation of the device.

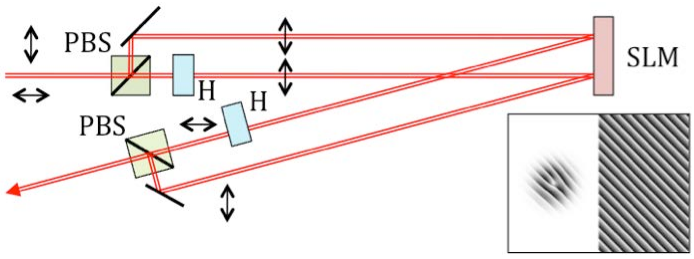

Figure 2. Polarization interferometer used to encode spatial modes according to polarization. Optical elements include polarizing beam splitters (PBS), half-wave plate (H) and spatial light modulator (SLM).

For all its virtues, the interferometer had to involve exactly equal paths to avoid decoherence. We then implemented the interferometer shown in Fig. 3, reported earlier in the year [20]. This is a Sagnac-type equal-path interferometer. The SLM was programmed to encode patterns in the specular reflection direction. The advantage of the interferometer of Fig. 3 is that it had immunity to vibrations and dephasings of a Sagnac interferometer, and did not introduce any decoherence. The interferometer had a clever manipulation of the polarization of the light.

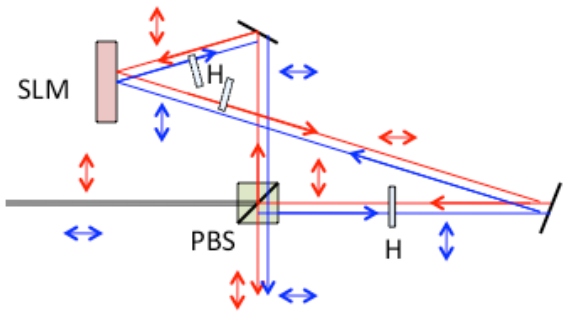

Figure 3. Sagnac-type interferometer used for immunity against decoherence. The interferometer used a polarizing beam splitter (PBS), spatial light modulator (SLM), and half-wave plates.

Properly placed half-wave plates insured that (i) the light entered through one port of the interferometer and exited the other one, (ii) sending vertically polarized light onto the SLM so that a spatial mode was encoded onto it, and (iii) the light exiting the interferometer preserved the incident linear polarization states of the light. The disadvantages of the interferometer of Fig. 3 were that it occupied space and required delicate alignment.

Whereas the interferometer of Fig. 3 was the solution to the decoherence problems, we devised a simpler and equally efficient interferometer. It is shown in Fig. 4. It takes advantage of the polarization sensitivity of the SLM by programming the light in two passes. It could be done with only one SLM, but we show our design using two SLMs. The vertical component of the light is encoded on the first SLM on specular direction while the spatial mode of the horizontal component is undisturbed. The polarization of the light is subsequently rotated by 90 degrees by a half-wave plate. This way, the second SLM encodes the polarization component that was reflected by the first SLM, and reflects the mode that was encoded by the first SLM.

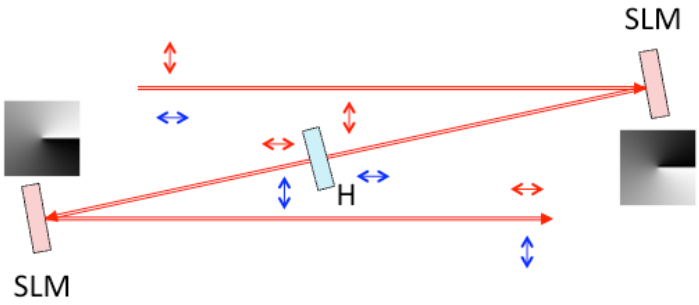

Figure 4. Same-path interferometer apparatus to entangle polarization and spatial mode. Optical elements include a half-wave plate (H) and a spatial light modulator (SLM). Image inserts are examples of the phase encoding to encode spatial modes $\ell = +1$ with horizontal polarization, and $\ell = -1$ with vertical polarization.

The operation effected by the interferometer can be represented by:

$$c_1|H,u_{00}\rangle + c_2|V,u_{00}\rangle \xrightarrow{SLM_1} c_1|H,u_{00}\rangle + c_2|V,u_{10}\rangle, \quad (13)$$

$$c_1|H,u_{00}\rangle + c_2|V,u_{10}\rangle \xrightarrow{HWP} c_1|V,u_{00}\rangle + c_2|H,u_{10}\rangle, \quad (14)$$

and

$$c_1|V,u_{00}\rangle + c_2|H,u_{10}\rangle \xrightarrow{SLM_2} c_1|V,u_{01}\rangle + c_2|H,u_{10}\rangle \quad (15)$$

Because both polarization components are part of the same beam, the interferometer is immune to decoherence. The simplicity and the apparatus of Fig. 4 make it an excellent device to use for encoding polarization-spatial modes.

3.3 Non-separable polarization-spatial states of single photons

The next step in implementing the polarization-spatial non-separable states of single photons was to perform a new type of experiment: demonstrating position-dependent polarization mode of single photons. This experiment, a first of its kind, was implemented with the apparatus of Fig. 5. Vertically polarized photon pairs were produced via type-I parametric down-conversion by a single BBO crystal. As mentioned earlier, the state of the light after the crystal is

$$|\psi\rangle = \sum_\ell c_\ell |V,u_\ell\rangle_1 \, |V,u_{-\ell}\rangle_2 \quad (16)$$

We used a single-mode fiber to project the spatial mode of photon 2 onto the fundamental $\ell = 0$ mode

$$|\psi'\rangle = |V,u_{00}\rangle_1 |V,u_{00}\rangle_2. \quad (17)$$

That is, due to the spatial mode entanglement, the spatial state of both photons was projected to the fundamental mode by passage of one of the photons through a single-mode fiber.

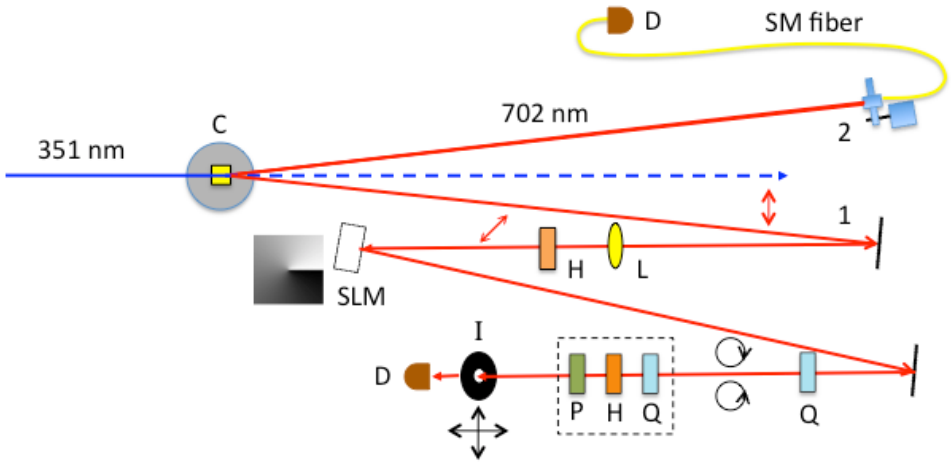

Figure 5. Schematic of the apparatus to measure the Poincare mode of a single photon. Optical elements include: BBO crystal (C), single-mode (SM) fiber, photon detectors (D), lens (L) half-wave plate (H), quarter-wave plate (Q), polarizer (P), spatial light modulator (SLM), and scanning iris (I). Elements within the dashed rectangle constitute a polarizing filter. The position of the iris is scanned in a 2-dimensional plane to provide a single-photon image of the transverse intensity profile of the photon.

The signal photon is imaged onto the SLM before passing through a half-wave plate, leaving the single photon in state

$$|\psi\rangle_1 = {}^1\!/_{\sqrt{2}}(|V,u_0\rangle + |H,u_0\rangle). \tag{18}$$

The SLM only encodes a mode onto the vertically polarized component, putting the photon in the state

$$|\psi'\rangle_1 = {}^1\!/_{\sqrt{2}}(|V,u_1\rangle + |H,u_0\rangle), \tag{19}$$

which is a non-separable state of polarization and spatial mode. We go further and convert to the circular polarization basis via a quarter-wave plate, leaving the light in the state:

$$|\psi''\rangle_1 = {}^1\!/_{\sqrt{2}}(|R,u_1\rangle + |L,u_0\rangle), \tag{20}$$

where the labels *R* and *L* represent right and left handed circular polarization. The light proceeds to a section of the apparatus where we perform imaging polarimetry. This entails taking six single photon images, pixel by pixel, after the passage through six different polarization filters, projecting the polarization state of the light at each point in the horizontal linear (*H*), vertical linear (*V*), diagonal linear (*D*), anti-diagonal linear (*A*), right circular (*R*), and left circular (*L*). From these six measurements we obtain the normalized Stokes parameters for each point:

$$s_1 = (N_H - N_V)/N_0, \tag{21}$$

$$s_2 = (N_D - N_A)/N_0, \tag{22}$$

$$s_3 = (N_R - N_L)/N_0, \tag{23}$$

where N_H, N_V, N_D, N_A, N_R, and N_L are the photon counts after each filter and N_0 is the total photon count before the filters. From these we can obtain the state of polarization of the light at each point, namely the ellipticity

$$\epsilon = \pm b/a = \tan\left(\frac{1}{2}\sin^{-1} s_3\right), \tag{24}$$

where b and a are the semi-minor and semi-major axes of the polarization ellipse; and the ellipse orientation

$$\theta = \frac{1}{2}\tan^{-1}\frac{s_2}{s_1}. \tag{25}$$

There are two more stages left in our quest. The stage that is currently underway is a tomography of this 2-qubit or ququart state. The expected outcome is a measurement of the density matrix of the state of the photon. We are also planning to prepare a three-dimensional state, a spatial qutrit, and entangle it with polarization, forming a ququint. The following stage is to replicate the action with the other photon, to implement the 2-photon cluster state.

3.4 Polarization singularities of polarization-spatial modes

Our research on the production of polarization-spatial modes led us to investigate the classical patterns produced by such modes. We found that laboratory studies of this problem had been very limited, so we initiated studies of this problem, in parallel to the quantum optics problem. We first define a general state of polarization in terms of the right and left circularly polarized states

$$\hat{e} = \cos\chi\ e^{i\theta}\ \hat{e}_R + \sin\chi\ e^{-i\theta}\ \hat{e}_L\ . \tag{26}$$

This basis is convenient because the polarization ellipse's ellipticity and orientation are decoupled from each other as shown by the left side of Fig. 6, and with χ related to the ellipticity by

$$\varepsilon = \tan\left(\pi/4 - \chi\right). \tag{27}$$

This formalism is also convenient for making connections with the Poincare sphere, where 2χ is the polar angle and 2θ is the azimuthal angle, as shown in Fig. 6.

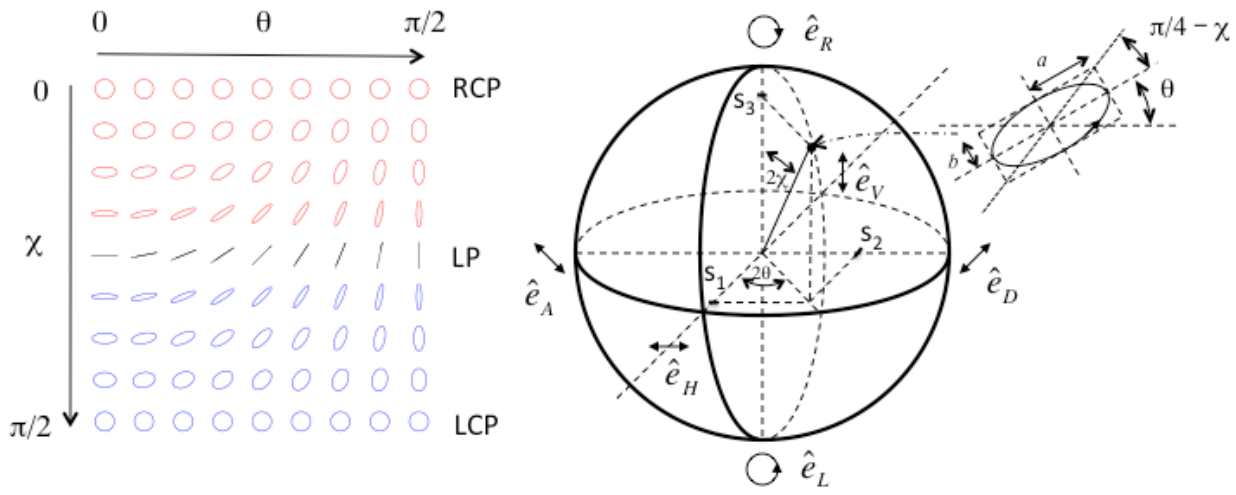

Figure 6. Mapping of the states of polarization to the Poincare sphere. The angles used in the representation of Eq. (26) are useful in mapping to the sphere and for specifying independently the characteristics of the polarization ellipse.

If we prepare an optical beam in a superposition of Laguerre-Gauss spatial modes in orthogonal states of polarization – a non-separable state of polarization and spatial mode, the expression for the amplitude of the mode is [21,22]

$$\hat{V} = {}^{1}/_{\sqrt{2}}\left(LG_{p_1}^{\ell_1}\, e^{i\alpha}\, \hat{e}_R + LG_{p_2}^{\ell_2}\, e^{-i\alpha}\, \hat{e}_L\right), \tag{28}$$

Where LG_p^{ℓ} represents the Laguerre-Gauss function with radial index p and azimuthal index ℓ (which also corresponds to the topological charge). If we replace the expression for the Laguerre-Gauss mode (with $p = 0$) and arrange it to be of the form of Eq. (26), we get very interesting expressions for the angles:

$$\chi = \tan^{-1} A_2 r^{|\ell_1|}, \tag{29}$$

where A_1 and A_2 are constants for each mode, and r is the transverse radial coordinate; and

$$\theta = \frac{1}{2}(\ell_1 - \ell_2)\phi + \alpha, \tag{30}$$

with ϕ being the transverse spatial coordinate. Equation (29) implies that the ellipticity of the state depends on r, and Eq. (30) implies that the orientation depends on ϕ. Thus, the mode of Eq. (28) corresponds to a mapping of the Poincare sphere onto the transverse beam profile. For this reason these type of modes are called Poincare modes [23]. Figure 7 shows the polarization maps of two beams, one with $\ell_1 = 1$ and $\ell_2 = 0$, and the other one with $\ell_1 = -1$ and $\ell_2 = 0$. The color denotes the handedness of the state of polarization.

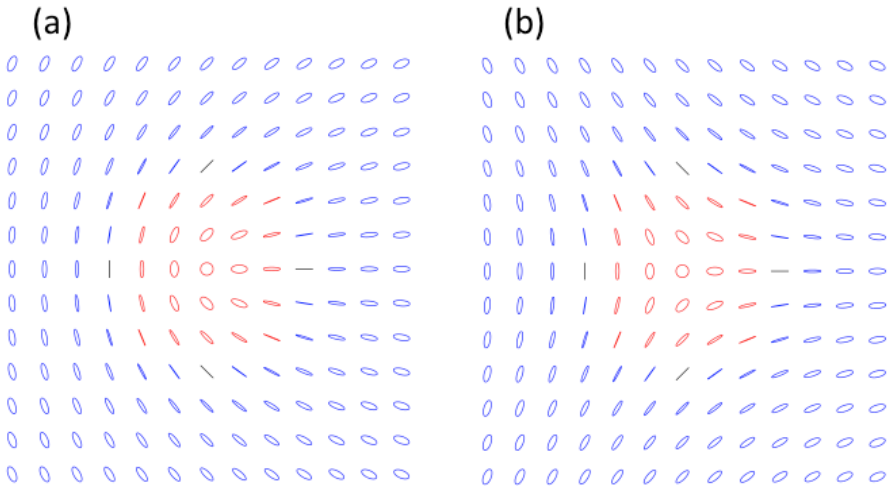

Figure 7. Map of the polarization ellipses in two types of Poincare modes (with $p = 0$), one with $\ell_1 = 1$ and $\ell_2 = 0$, and the other one with $\ell_1 = -1$ and $\ell_2 = 0$ (see equation 28).

The center of both patterns in Fig. 7 are polarization singularity C-points. These are points of circular polarization that are surrounded by states of elliptical polarization with orientation that rotate about the C-point. The pattern in Fig. 7(a) is known as a lemon. The orientation of the ellipses in the field is given by

$$\theta_L = +\phi/2 \tag{31}$$

Similarly, the pattern of Fig. 7(b), known as a star, has

$$\theta_S = -\phi/2. \tag{32}$$

In both cases the orientation of the ellipse is independent of r, so the point $r = 0$ (i.e., the C-point) is a singular point, where orientation is undefined.

Given the potential of Eq. 28, we embarked in measuring these modes classically. We did so with two setups. Figure 2 has the most recent one, which uses an SLM to encode the modes [24]. The only difference is that to make the modes of Eq. (28) we need to be in the circular basis, which requires the addition of a quarter-wave plate.

3.5 Creating asymmetric singularities, and finding the monstar.

Our study of Poincare beams led us to the implementation of polarization-spatial modes that produced the classical patterns of Fig. 7. These C-points are symmetric and have been produced in isolation in optical beams by other groups [23,25]. However, theoretical studies predict a much more general type of C-point that is asymmetric [26,27,28], and which contains a third kind of C-point known as the monstar. The three types of C-points are presented in Fig. 8. The lines in the figure are tangent to the semimajor axis of the ellipses, and so provide a grasp of the topology of the ellipse field. In fact, these polarization lines have an analogy to the topology of

surfaces [29], where they represent lines of curvature, which are tangent to the principal axes of curvature of a surface. The C-point is the umbilic, or the point where the principal curvatures are the same, and the surface curvature is therefore spherical. Figure 8 shows the cases of the three types of umbilics.

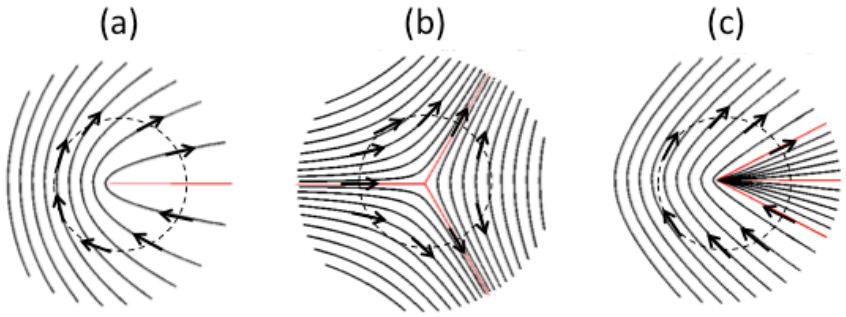

Figure 8. Polarization lines for the three types of C-points, lemon (a), star (b) and monstar (c). Radial polarization lines are shown in red.

The key distinctions of the patterns of Fig. 8 are:

(i) The sense of rotation of the ellipses for a path about the C-point, and

(ii) The number of directions where the lines are radial.

Arrows placed along the circular path in Fig. 8 show this. The lemon of case (a) has arrows rotate counter-clockwise for a counter-clockwise path, and one radial line. The star of case (b) is distinct: clockwise rotation for a counter-clockwise path and three radial lines. Case (c), has the same rotation as the lemon and the same number radial lines as the star, thus it is called (le)monstar.

4.0 RESULTS AND DISCUSSION

4.1 Polarization entanglement of photons in the fundamental spatial mode

The setup of Fig. 1 entails the production of polarization-entangled photons in the state of Eq. (1). The spatial state is still in a superposition of spatial modes of Eq. (3). The apparatus further projects the spatial mode by passage through single-mode fibers. Beyond this point, the plan was to encode spatial modes.

Our first step in the process was to diagnose the state of the light past the single-mode fibers. We did this with the apparatus of Fig. 9. We found that the fibers modified the polarization state of the light, and so transforming the quantum state of Eq. (1) into an undesired state. We investigated using polarization-maintaining optical fibers to preserve the state, but we found that while the state of polarization was preserved, the collection efficiency was much decreased from that of non-polarization-maintaining single-mode fibers. Thus, we switched back to plain single-mode fibers. Our procedure was then to undo the polarization transformations effected by the fiber by adding a set of waveplates after the fiber, as shown in the figure. The unitary transformation that the fiber applied due to its birefringence was reversed by the waveplates.

Once this was done successfully, we did successfully diagnose the state of the light, showing polarization entanglement after the single-mode fibers.

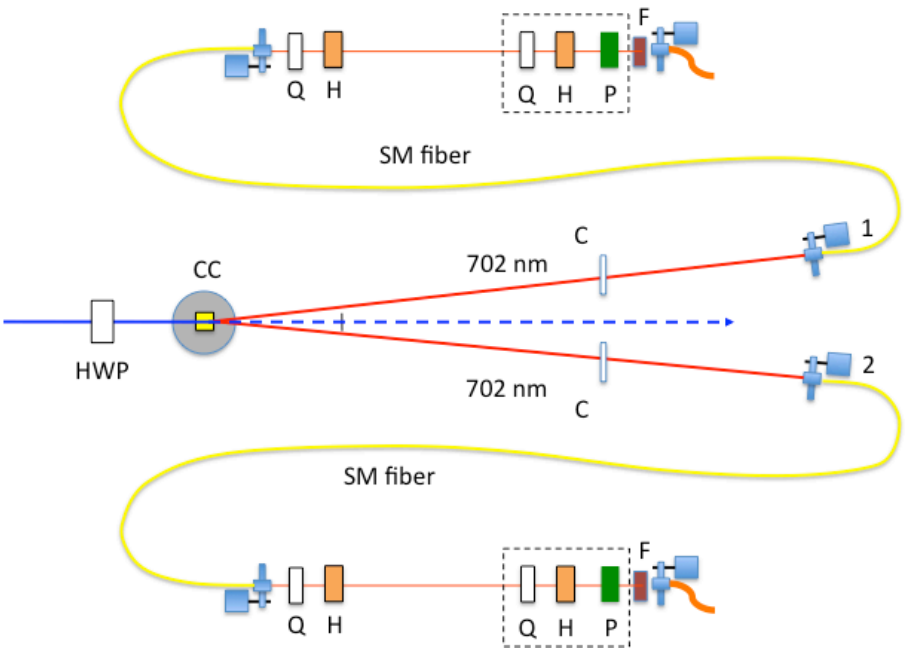

Figure 9. Schematic of the apparatus to test the polarization entanglement past the single-mode fibers. The optical elements within the highlighted rectangle provided polarization filters. Optical elements are half-wave plate (H), quarter-wave plate (Q), polarizer (P), BBO crystal (CC) and single-mode fiber (SM).

4.2 Encoding of spatial modes with spatial light modulators

An important aspect of the project was the use of SLMs for encoding the spatial mode onto single photons. We developed Matlab programs to do this. In addition, to encode a superposition of modes we programmed the SLM to encode distinct modes on adjacent parts of the SLM.

Figure 10 shows an example of the programming of the SLM to produce adjacent beams in distinct spatial modes. The patterns encode in gray scale the phase that is imparted onto the light beams. The patterns are diffraction gratings with a phase blaze. For the patterns shown in the figure we reduced the density of lines by a factor of 10. The actual patterns had a density of about 14 lines/mm, diffracting the light at an angle of about 0.5 degrees. The left and right panes of Fig. 10 encoded Laguerre-Gauss spatial modes with topological charges 1 and 2, respectively. The dislocation seen in the center of the patterns gathers this: preparing a mode with topological charge ℓ required a diffraction pattern with a fork with $\ell + 1$ tines. The patterns were amplitude modulated to optimize the generated mode. This so because light diffracted off the actual

dislocation produced diffraction rings. By changing the blazing of the phase in the center of the fork we eliminated the rings and maximized the purity of the mode that was generated. The patterns of Fig. 10 encoded the modes on first order diffraction. The apparatus of Fig. 2 generated the adjacent beams and combined the diffracted beams to form non-separable modes of polarization and spatial mode.

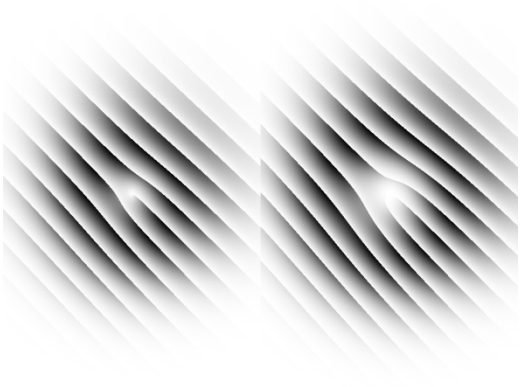

Figure 10. Programming of the SLM for preparing adjacent beams in distinct spatial modes. The gray scale is proportional to the phase imparted, with 0 = white and 2π = black. The left and right panes encode Laguerre-Gauss modes with topological charges 1 and 2, respectively.

Whereas the patterns of Fig.10 encoded modes on first-order diffraction for use with the apparatus of Fig. 2, the pattern of Fig. 11 encoded spatial mode on zero-order (i.e., at the specular angle), for use in the apparatuses of Figs. 3, 4 and 5.

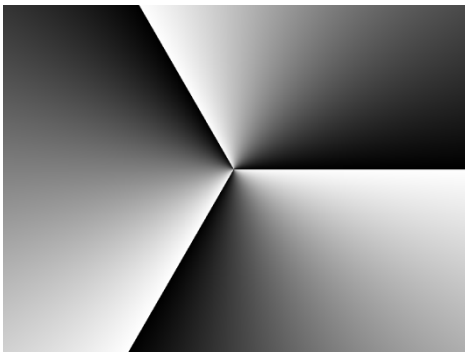

Figure 11. Pattern programmed onto the SLM for imparting a spatial mode on reflection. The gray scale is proportional to the phase imparted, with 0 = white and 2π = black. The pattern encoded a Laguerre-Gauss mode with topological charge 3.

The same type of programming is used to decode the mode. This method converts a certain spatial mode onto a fundamental mode. The light is then focused onto a single-mode fiber that acts as a fundamental mode filter [5].

4.3 Characterizing polarization-spatial modes of photons

As mentioned earlier, our investigations of polarization-spatial modes led us to the implementation of a novel type of optical beams, Poincare beams, where the state of polarization varies from point to point in the transverse profile. These beams contain all the states of polarization. We prepared these beams with polarization interferometers. Our first interferometers used passive diffraction gratings to encode the modes, and the second generation of experiments used SLMs to encode the modes. We diagnose the modes in two ways: by polarization-state nulling [21,22] and by imaging polarimetry [24].

Figure 12 shows the result of state nulling measurements in diagnosing the mode of a Poincare beam bearing a star C-point singularity [12]. Our apparatus sent the light through a set of polarization filters set to null a particular polarization state, followed by a digital camera, as shown in Fig. 12(c).

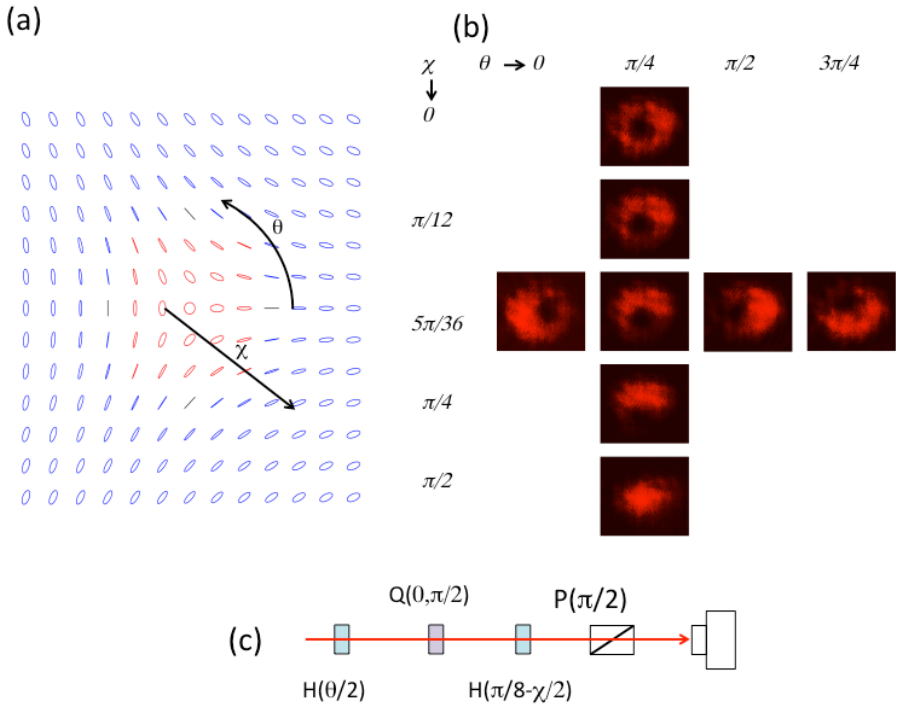

Figure 12. Measurements of the star mode of a Poincare beam by state nulling. The predicted pattern of polarization is shown in (a), the nulling measurements are shown in (b), and the nulling apparatus is shown in (c).

The nulling filter selected the polarization state by the angles χ and θ, which specified the ellipticity and orientation, respectively, as explained in Sec. 3.4. For example, the images of Fig. 12(b) for $\theta = \pi/4$ (i.e., semimajor axis oriented by 45 degrees), have increasing value of χ. For $\chi = 0$ we are at the north pole of the Poincare sphere (see Fig. 6), and according to the pattern of Fig. 12(a), this state should be at the center of the beam. Indeed the corresponding image has a

dark spot in its center, consistent with nulling that state. As χ is increased, the ellipticity of the selected state decreases. This is equivalent to traveling along a meridian of the Poincare sphere of Fig. 6 toward the south pole. The ellipticity of the ellipses oriented by $\theta = \pi/4$ in the pattern of Fig. 12(a) decreases from the center of the beam downward. Indeed, the same is seen in the measured images: the dark spot moves to lower positions in the beam as χ of the filter is increased.

A second form of diagnosis involved a different approach, described in Sec. 3.3, involved imaging polarimetry. It entails taking six images with six polarization filters, and extracting from them the state of polarization of each point. Figures 13(b) and 13(c) show our imaging polarimetry diagnosis of the pattern of Fig.13(a), which is the same pattern as Fig. 12. The color denotes the orientation of the polarization. The measured patterns agree quite well with the expected patterns.

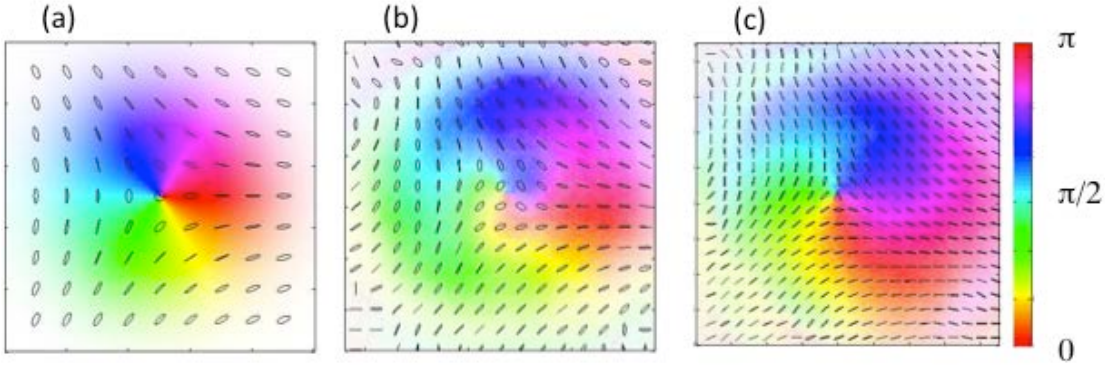

Figure 13. Poincare patterns measured by imaging polarimetry. The predicted (a), and measured (b) and (c), patterns of a star C-point are shown. The color represents orientation of the state of polarization and its saturation is proportional to the intensity.

The measurements of Fig. 13(b) were done on modes generated with the setup of Fig. 2, whereas the one in Fig. 13(c) were done with the new apparatus of Fig. 4 (without the second SLM). We can see a marked improvement in the uniformity of the patterns in Fig. 13(c) over those of Fig. 13(b). The patterns in Figs. 13(b) and 13(c) were taken in different days and not for the purpose of comparison. They also encode a slightly different phase that makes them appear rotated relative to each other, but that is a minor experimental effect that is easily varied.

4.4 Creating and diagnosing asymmetric C-points

Since asymmetric C-points had not been produced in isolation in optical beams before, we embarked on generating them. More recent theoretical work on the problem presented a two dimensional planar space as the space where all the C-points can be mapped [28]. We found a more accurate description: a spherical shell, shown in Fig. 13.

Our solution to the problem of generating an asymmetric C-point was to consider the essence of a C-point: an optical vortex in a state of circular polarization superimposed by a plane wave in the opposite state of circular polarization. When the optical vortex is a pure one, the C-point is symmetric. The symmetric lemon and star C-points are generated by the superposition

$$\hat{V}_{\text{sym}} = {}^{1}/_{\sqrt{2}}\left(LG_0^{\pm 1}\,\hat{e}_R + LG_0^0\,\hat{e}_L\right) \tag{33}$$

where the plus corresponds to a lemon and the minus to a star. The pure Laguerre-Gauss modes have a uniformly varying phase, leading to ellipse orientations in the C-points given by the linear relations of Eqs. (30) and (31). Our past experience with mode superpositions [30] led us to the solution of the problem: to create asymmetric C-points we need asymmetric vortices created by superpositions of vortices with opposite topological charge:

$$\hat{V}_{\text{asym}} = {}^{1}/_{\sqrt{2}}[(\cos\beta\, LG_0^{+1} + \sin\beta\, LG_0^{-1})\,\hat{e}_R + LG_0^0\,\hat{e}_L]. \tag{34}$$

New parameters that we added are β to account for the relative weights of the two vortices and γ to account for their relative phase. An additional phase δ accounts for the relative phase between

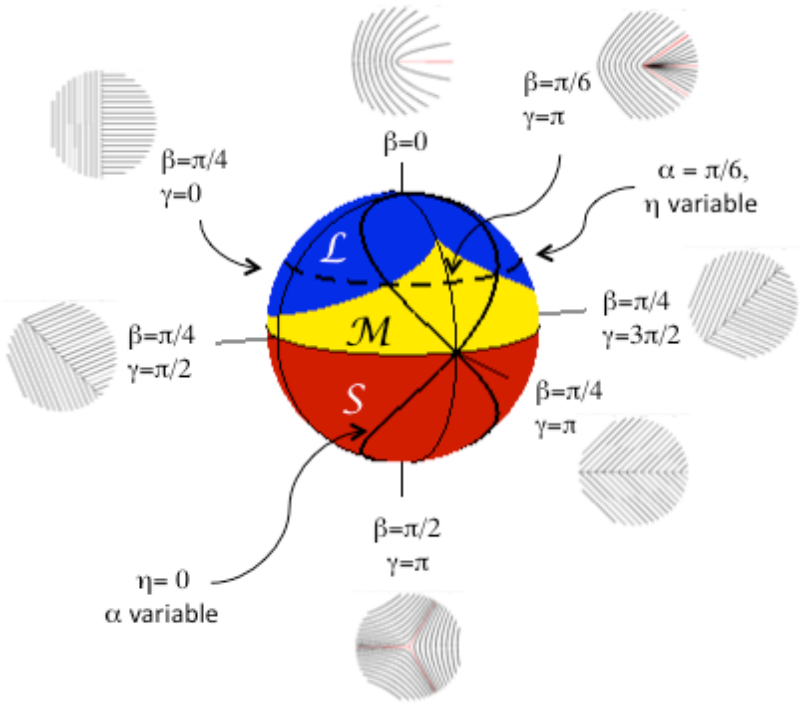

Figure 14. Sphere mapping polarization singularity C-points. Colored regions denote the three different types of C-points: lemon (L), monstar (M) and star (S). Inserts are the polarization-line patterns.

the two polarization components. When $\delta = 0$ the space of modes is mapped onto a sphere (Fig. 14), similar to the Poincare sphere, with 2β being the polar angle and γ the azimuthal angle.

Since the Laguerre-Gauss expressions in Eq. (33) are functions of the transverse coordinates, we can use Eq. (33) to identify all the types of C-point patterns [24,31,32]. We note that the quantum state corresponding to Eq. (33) uses a non-separable superposition of 3 spatial modes (a qutrit)

with two polarization modes (a qubit), thus constituting a 5-dimensional quantum state, a ququint.

Once we determined the theory involving the generation of all types of C-points we proceeded to generate and measure them in the laboratory with a setup that was very similar to Fig. 2. Figure 15 shows our data that has been submitted for publication [32]. The data shows the simulations and measurements of the optical beams bearing isolated C-points for different values of the parameter β. The ones for $\beta = 0^\circ$ and $\beta = 90^\circ$ correspond to the symmetric lemon and star, respectively. The ones for $\beta = 30^\circ$ and $\beta = 40^\circ$ correspond to monstars. Our measurements are the first reporting the creation of isolated monstars.

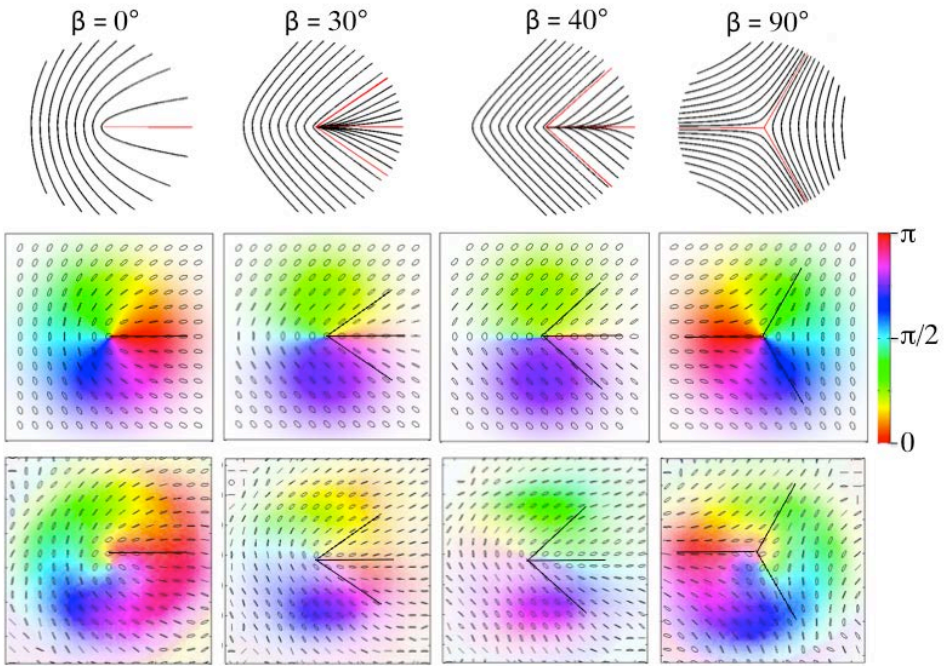

Figure 15. Theory and measurements of isolated asymmetric C-points. The first row shows the polarization-line maps for several values of β, $\gamma = \pi$ and $\delta = 0$; the second one shows the predicted beam patterns, and the third row show the measured patterns. The solid lines in the second and third rows show the predicted position of the radial lines (red lines in the patterns of the first row).

The data of Fig. 15 is very good. We have much more data analyzing other intricacies of the problem, such as the patterns obtained by varying γ and δ. Those parameters destroy the remaining symmetry (about the horizontal axis in Fig. 15), and rotate the patterns.

In addition to our measurements, we connected with a research group at the University of Hyderabad, who have done similar measurements but via superpositions of Hermite-Gauss modes. We worked out the correspondence between the two approaches, yielding an equation similar to Eq. (33) but with Hermite-Gauss modes. The correspondence between the two

approaches is related to the figure-8 inscribed on the sphere of Fig. 14, which is described in the article submitted for publication.

In addition, we have started taking data with the new and improved setup of Fig. 4, obtaining even better results (see next section). This work is still in progress.

4.5 Single photons in non-separable 2-qubit polarization-spatial states

C-points are a novel optical mode that has not been measured at the single photon level. It underscores the mystery that is the photon, not only being in a mode that can have distinct phases and amplitudes in its profile, but in a mode that has all states of polarization in its profile. A measurement of this type of mode is a milestone in our understanding of what light is.

We used the setup of Fig. 5 to make this measurement. It prepared the light in the heralded single-photon state of Eq. (19). We then took single-photon images, pixel by pixel, with the six polarization filters to determine the state of polarization of each pixel. Figure 16 show our best preliminary data, as the work is still ongoing. As can be seen, the results are excellent. We show the two types of C-points that we can create with the non-separable state of two spatial modes and two polarization states.

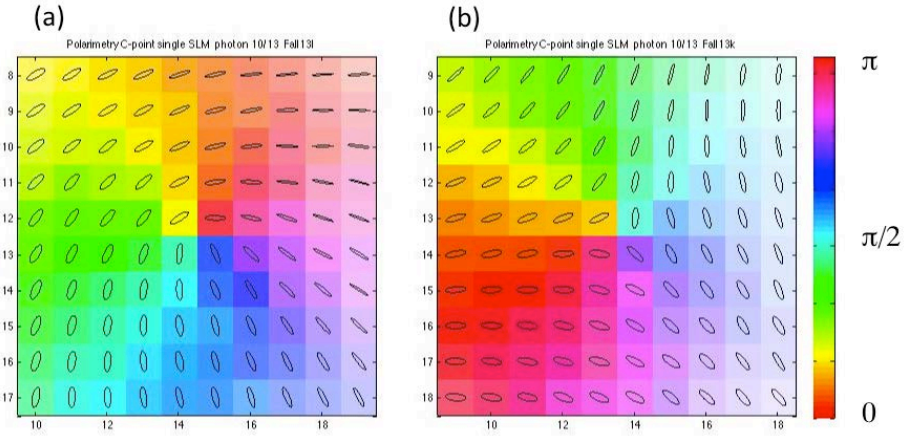

Figure 16. Results of the measurement of the C-point pattern of single photons, showing the lemon (a) and star (b) patterns.

We are currently taking more data on this to improve on the images shown. From the images it appears that there is an imbalance in amplitudes between the right-circular and left-circular components. Upon balancing, both patterns will exhibit all states of polarization. We also want to record images of monstars, which constitute adding a third dimension to the Hilbert space of spatial modes. That result will also be unique. We are close to achieving these objectives. They will be followed by a complementary tomographic measurement using a second SLM in the setup of Fig. 4.

4.6 Publications and Presentations

This grant produced the following publications:

1. "Preparing photon pairs entangled in any desired spatial modes via interference," E.J. Galvez, Proc. SPIE **8057**, 805706 1-5 (2011).
2. "Proposal to produce two and four qubits with spatial modes of two photons," E.J. Galvez, Proc. SPIE **8274**, 82740G 1-5 (2012).
3. "Poincare modes of light," E.J. Galvez and S. Khadka, Proc. SPIE **8274**, 82740Y 1-8 (2012).
4. "Poincaré-beam patterns produced by nonseparable superpositions of Laguerre–Gauss and polarization modes of light," E.J. Galvez, S. Khadka, W.H. Schubert, and S. Nomoto, Applied Optics **51**, 2925-2934 (2012).
5. "Imaging optical singularities: Understanding the duality of C-points and optical vortices," E.J. Galvez, B.L. Rojec, and K.R. McCullough, Proc. SPIE **8637**, 863706 (2013).
6. "Vector Beams in Free Space," E.J. Galvez in *Angular Momentum of Light*, D.L. Andrews and M. Babiker Eds. (Cambridge University Press, Cambridge, 2013).
7. "Polarization of Light Beams" in *Photonics Handbook* (Wiley, in press—expected Jan 2014).
8. "Generation of isolated asymmetric unbilics in light's polarization,'' E. J. Galvez, B.L. Rojec, V. Kumar and N.K. Viswanathan (submitted to Physical Review).
9. "C-point Singularities in Poincare Beams" E.J. Galvez, B.L. Rojec, K. Beach, and X. Cheng (to appear in Coherence in Quantum Optics X, 2014)

During this period we made the following presentations where funding by this grant was acknowledged:

1. "Topological umbilics of Poincare' mode polarization superpositions," invited talk at the International Conference on Correlation Optics, Chernivtsi, Ukraine, September 19, 2013.
2. "Polarization singularities in Poincare' optical beams," E.J. Galvez and B.L. Rojec, Iberoamerican Conference on Optics RIAO/Optilas, Porto, Portugal, July 24, 2013.
3. "Discovering monstars: Unraveling new coherent-optical landscapes of polarization amplitude and phase," Invited talk at the Tenth Conference on Coherence and Quantum Optics, Rochester, June 17, 2013.
4. "Polarization patterns and singularities of Poincare' beams," Invited talk at the Second International Conference on Optical Angular Momentum, Glasgow, Scotland, June 4, 2013.
5. "Beyond qubits with spatial modes of light," E.J. Galvez, M. Senatore, X. Cheng, and B.L. Rojec. Contributed talk at the conference of the SPIE Defense and Security, Baltimore, May 3, 2013.

6. "Production of two-photon cluster states in polarization and spatial modes,'' E.J. Galvez, W.H. Schubert and M. Senatore. Contributed talk at the conference of the SPIE Photonics West, San Francisco, February 6, 2013.
7. "Multipole polarization patterns in Poincare' beams," E.J. Galvez, B.L. Rojec and K. McCullough. Contributed talk at the conference of the SPIE Photonics West, San Francisco, February 5, 2013.
8. "Non-separable Spatial and Polarization modes" Invited talk at the New York Center for Complex Light Workshop. City College of New York, New York City, October 30, 2012.
9. "Polarization singularities on demand with Poincaré beams,'' International Conference on Singular Optics,'' Sevastopol, Ukraine, September 18, 2012.
10. "An Advanced Lab on Polarization Optics with Poincaré Beams," E.J. Galvez, Poster presentation at the Meeting of the AAPT, at U. Penn, Philadelphia, July 29, 2012.
11. "Vortex Party!" Invited talk at a Workshop on Optical Vortices, City College of New York, New York, July 19, 2012.
12. "Polarization singularities in Poincaré optical Gaussian beams," E.J. Galvez and S. Khadka, Contributed talk at the conference of the SPIE Photonics West, January 26, 2012.
13. "Two-photon cluster states using polarization and spatial modes,'' E.J. Galvez, M.V. Novenstern, and W.H. Schubert. Contributed talk at the conference of the SPIE Photonics West, January 25, 2012.
14. "Vector Beams and Making Entangled States of Spatial Modes," Invited talk at the Cross Border Cross-Border Workshop on Laser Science, Rochester, June 11, 2011.
15. "Polarization-Spatial-Mode Entanglement of Photon Pairs, International Conference on Quantum Information, Ottawa, Canada, June 6, 2011.
16. "Proposals to Produce Entangled States of Spatial Modes of Light," E.J. Galvez, M.W. Novenstern, S. Nomoto, and W.H. Schubert, SPIE Defense and Security, Orlando, April 28, 2011.

5.0 CONCLUSIONS

In summary, this work had the following outcomes:

- It enabled conceptual/theoretical plans for producing photon pairs entangled in polarization and any desired spatial mode.
- It developed techniques to encode spatial modes using SLMs in arrangements that were immune to decoherence.
- It provided new theoretical and measurements of the fundamentals of optical beams in non-separable superpositions of polarization and spatial mode. This work went on to develop a new type of beam modes, Poincare modes, which are novel.
- The work on classical polarization-spatial modes resulted in new advances in the field of singular optics, by providing the theoretical formalism and measurements of types of patterns that had not been observed before.

- The maturing of the understanding and the techniques developed were implemented in a first measurement of the polarization pattern of a single photon in a non-separable superposition of polarization and spatial mode.

The outcomes did not include our ultimate goal of making a cluster state of two photons in a cluster state of polarization and spatial mode. However, we moved deliberately toward that goal by developing techniques and theoretical formalisms. The methods that were developed are robust and the prospect of reaching our goal is a good one. In addition, the development of techniques that combine polarization and spatial mode have applications beyond quantum computation. As is the nature of research, some unexpected results can result in unanticipated consequences, such as applications in different fields. The combination of polarization and spatial mode promises interesting applications in the encoding and decoding of images with an additional degree of freedom than is currently the case.

6.0 REFERENCES

[1] D.A. Miller and E.L. Dereniak Appl. Opt. **51**, 4092 (2012).

[2] R.K. Erdmann, M.L. Fanto, P.M. Alsing, C.J. Peters, E.J. Galvez, and W.A. Miller, Proc. SPIE **8057**, 805707 1-13 (2011).

[3] M.L. Fanto, R.K. Erdmann, P.M. Alsing, C.J. Peters, and E.J. Galvez, Proc. SPIE **8057**, 805705 1-12 (2011).

[4] A. Aspect, P. Grangier, and G. Roger, Phys. Rev. Lett. **49**, 91 (1982).

[5] A. Mair, A. Vaziri, G. Weihs, and A. Zeilinger, Nature (London) **412**, 313 (2001).

[6] J.T. Barreiro, N.K. Langford, N.A. Peters, P.G. Kwiat, Phys. Rev. Lett. **95,** 260501 (2005).

[7] S.S.R. Oemrawsingh, X. Ma, D. Voigt, A. Aiello, E.R. Eliel, G.W. ’t Hooft, and J.P. Woerdman, Phys. Rev. Lett. **95**, 240501-1–4 (2005).

[8] J. Leach, B. Jack, J. Romero, M. Ritsch-Marte, R.W. Boyd, A.K. Jha, S.M. Barnett, S. Franke-Arnold, and M.J. Padgett, Opt. Express **17**, 8287–8293 (2009).

[9] E. Nagali, F. Sciarrino, F. De Martini, L. Marrucci, B. Piccirillo, E. Karimi, and E. Santamato, Phys. Rev. Lett. 103, 013601-1–4 (2009).

[10] G. Molina-Terriza, J.P. Torres, and L. Torner, Nature (London) **3**, 305 (2007).

[11] Q. Zhan, Adv. Opt. Photon. **1**, 1 (2009).

[12] E.J. Galvez in *Angular Momentum of Light*, D.L. Andrews and M. Babiker Eds. (Cambridge University Press, Cambridge, 2013).

[13] C. Maurer, A. Jesacher, S. Fürhapter, S. Bernet, and M. Ritsch-Marte, New J. Phys. **9**, 78 (2007).

[14] J.F. Nye, *Natural focusing and fine structure of light: caustics and wave dislocations*, (Institute of Physics Publishing, Bristol) 1999.

[15] J. F. Nye, Proc. R. Soc. London Ser. A **389**, 279 (1983).

[16] J.P. Torres, Y. Deyanova, L. Torner, and G. Molina-Terriza, Phys. Rev. A **67**, 052313 (2003).

[17] E.J. Galvez, Proc. SPIE **8057**, 805706 1-5 (2011).

[18] E.J. Galvez, Proc. SPIE **8274**, 82740G 1-5 (2012).

[19] P.G. Kwiat, E. Waks, A.G. White, I. Appelbaum, and P.H. Eberhard, Phys. Rev. A **60**, 773 (1999).

[20] R. Fickler, R. Lapkiewicz, W.N. Plick, M. Krenn, C. Schaeff, S. Ramelow, A. Zeilinger, Science **338**, 640 (2012).

[21] E.J. Galvez, S. Khadka, W.H. Schubert, and S. Nomoto, App. Opt. **51**, 2925 (2012).

[22] E.J. Galvez and S. Khadka, Proc. SPIE **8274**, 82740Y (2012).

[23] A. M. Beckley, T. G. Brown, and M. A. Alonso, Opt. Express **18**, 10777 (2010).

[24] E.J. Galvez, B.L. Rojec, and K.R. McCullough, Proc. SPIE **8637**, 863706 (2013).

[25] F. Cardano, E. Karimi, L. Marrucci, C. de Lisio, and E. Santamato, Opt. Express **21**, 8815 (2013).

[26] M. V. Berry and M. R. Dennis, Proc. Roy. Soc. Lond. A **457**, 141 (2001).

[27] M. R. Dennis, Opt. Commun. **213**, 201 (2002).

[28] M.R. Dennis, Opt. Lett. **33**, 2572 (2008).

[29] M. V. Berry and J. H. Hannay, J. Phys. A **10**, 1809 (1977).

[30] S. M. Baumann, D. M. Kalb, L. H. MacMillan, and E. J. Galvez, Opt. Express **17**, 9818 (2009).

[31] E.J. Galvez, B.L. Rojec, K. Beach, and X. Cheng (to appear in Coherence in Quantum

Optics X, 2014)

[32] E. J. Galvez, B.L. Rojec, V. Kumar and N.K. Viswanathan (submitted for publication).

7.0 LIST OF SYMBOLS, ABBREVIATIONS, AND ACRONYMS

BBO: Beta barium borate

HG: Hermite-Gauss

LG: Laguerre-Gauss

SLM: Spatial light modulator